https://doi.org/10.31436/iiumej.v26i1.3157

MAP FLOODWATER RADAR IMAGERY USING MACHINE LEARNING ALGORITHMS

THANH NGHI DOAN[1,2], DUC-NGOC LE-THI[1]

[1]*Faculty of Information Technology, An Giang University, An Giang, Vietnam*

[2]*Vietnam National University, Ho Chi Minh City, Vietnam*

**Corresponding author: dtnghi@agu.edu.vn*

(Received: 7 January 2024; Accepted: 10 October 2024; Published online: 10 January 2025)

ABSTRACT: Flooding is a widespread and costly natural disaster around the world. Accurately assessing the extent of flooding in near real-time is crucial for governments and humanitarian organizations. This information strengthens early warning systems, evaluates risks, and guides effective relief efforts. Therefore, precise flood mapping is essential for saving lives through improved early warning systems and targeted emergency responses. In this study, radar imagery available on the Planetary Computer Data was utilized to train a U-Net model specifically designed to label flood-affected pixels in an image from a flood event. Different blocks of the U-Net encoder architecture were fine-tuned to identify the most efficient fine-tuned model, and their results were compared. As a result, the model with blocks 1 and 2 being fine-tuned demonstrated the highest Intersection over Union (IoU) score of 78.904%, an increase of 8.663% over the baseline methods.

ABSTRAK: Banjir merupakan bencana alam yang meluas dan mahal di seluruh dunia. Penilaian yang tepat terhadap skala banjir secara hampir masa nyata adalah penting bagi kerajaan dan organisasi kemanusiaan. Maklumat ini memperkukuhkan sistem amaran awal, menilai risiko, dan membimbing usaha bantuan yang lebih berkesan. Oleh itu, pemetaan banjir yang tepat adalah penting untuk menyelamatkan nyawa melalui sistem amaran awal yang lebih baik dan respons kecemasan yang disasarkan. Dalam kajian ini, imej radar yang tersedia pada Planetary Computer Data digunakan untuk melatih model U-Net yang direka khas untuk melabelkan piksel yang terjejas oleh banjir dalam imej daripada kejadian banjir. Bagi mengenal pasti model ditala-halus yang paling cekap, blok-blok berlainan dalam arkitektur pengekod U-Net telah ditala-halus, dan hasilnya dibandingkan. Hasilnya, model dengan blok 1 dan 2 yang ditala-halus menunjukkan skor Intersection over Union (IoU) tertinggi sebanyak 78.904%, iaitu peningkatan sebanyak 8.663% berbanding kaedah asas.

KEYWORDS: *Flood mapping, Fine-tunning, Radar imagery, U-Net*

1. INTRODUCTION

Floods are natural disasters when large amounts of water temporarily submerge land. According to [1], strategies to mitigate the effects of floods can be broadly categorized into two types: prevention measures and complementary solutions. Prevention measures focus on infrastructure and physical interventions to control water flow and reduce water accumulation [2]. Complementary solutions, which work in tandem with prevention efforts, aim to enhance flood management [3]. These include flood monitoring, early warning systems, emergency response protocols, and public awareness campaigns. Among these, early warning systems are particularly effective, as they provide timely and accurate information about the extent of the

affected area in advance. This enables better damage assessment and mapping, aiding crisis management and recovery.

Various methods have been explored for mapping floods and assessing flood risks. Traditional approaches, such as those mentioned in [4], have been commonly used to address these challenges. While high-resolution hydrologic models are effective at smaller scales, their application to community-level urban flooding is limited by high computational and data input requirements [5]. This underscores the need for innovative techniques to predict flooding accurately without demanding extensive computational resources.

Remote sensing, particularly Synthetic Aperture Radar (SAR), provides an efficient and cost-effective solution for large-scale flood mapping without the need for highly accurate or resource-intensive processes. Unlike traditional methods that often face challenges in addressing the complexities of urban flooding, SAR offers a more robust alternative. A detailed examination of remote sensing techniques, including SAR and multi-frequency Polarimetric SAR for terrain classification, is presented in [6]. As an active sensor, SAR excels at capturing detailed images of the Earth's surface, regardless of time of day or cloud cover. Its capabilities have greatly improved flood detection and monitoring.

For instance, in [7], innovative multi-temporal COSMO-SkyMed data from Northern Italy were utilized to develop a classification algorithm for mapping flood progression. The authors in [3] demonstrated the successful use of RADARSAT-2 SAR images and flood stage data to monitor the 2011 Richelieu River flood. Additionally, the study in [8] combined TerraSAR-X with high-resolution aerial imagery to capture the complex flooding dynamics along the River Severn in England.

Recently, significant advancements have been made in supervised machine learning algorithms, particularly in deep learning techniques and Convolutional Neural Networks (CNNs) [9]Unlike traditional pixel-based learning methods, CNNs exploit the spatial structure of target segments, enabling more effective feature extraction. Additionally, automatic feature representation within CNNs partitions the feature space, reducing uncertainties in the data. Due to these capabilities, CNNs have emerged as powerful tools in various fields, with recent successes in flood mapping being a prime example.

In 2019, the authors of [10] investigated using CNNs for flood detection from high-resolution unmanned aerial vehicle (UAV) images. They employed a VGG-based fully convolutional network (FCN-16s). They demonstrated that CNNs outperformed traditional classification methods, such as fully convolutional networks (FCNs) and support vector machines (SVMs), in identifying flooded regions. In another study, the authors of [11] developed a CNN-based approach specifically for extracting flooded areas from Sentinel-1 SAR data. Their method involved generating flood masks through classical semi-automatic techniques, followed by manual cleaning and visual inspections, while exploring different CNN architectures. This approach significantly reduced the time needed to produce flood maps. The CNN models used in the study achieved impressive F1 scores of 91% and 92% on the test dataset.

Nevertheless, training a deep convolutional neural network from scratch presents substantial challenges, particularly in fields like medical imaging, where annotated data is often limited and expensive to obtain. A promising alternative is transfer learning, which involves fine-tuning a pre-trained network for a specific application. This approach adapts a network trained on a large, general dataset to a new task. When working with a small dataset, it is typically recommended to retain the initial layers of the pre-trained network and fine-tune only the final layers for the new application [12]. The authors in [13] propose a deep learning-based

flood detection system using semantic segmentation with a U-Net architecture to analyze aerial and satellite images, detecting flood-affected regions at the pixel level. Trained on a diverse set of annotated flood images, the model achieves an IoU score of 0.85, surpassing existing methods in accuracy. This system offers real-time flood mapping, enhancing disaster response by providing timely, accurate data, which helps emergency responders assess the extent of the disaster, plan rescue operations, and manage resources more effectively.

The authors in [14] provides a reasoned overview of flood detection using SAR imaging. The main detection mechanisms, such as thresholding and machine learning-based algorithms, and the usual performance measures used to assess the reliability of demarcation maps have been reviewed. The presentation included publicly accessible SAR datasets with accompanying reference labeled data that may be utilized for both performance assessment and ML algorithm training. Situations where SAR-based flood detection remains difficult, such as in the presence of vegetation, terrain, or metropolitan areas, have been considered. They finish this assessment by discussing future viewpoints on the subject.

The U-Net model [15], widely recognized for its speed and accuracy in medical image segmentation, has also been successfully applied to SAR image segmentation [16], [17]. In particular, the study by [18] demonstrated that the U-Net model outperforms the X-Net model in flood detection using radar imagery from both polarizations. For Vertical-Horizontal (VH) polarization, the U-Net model achieved an Intersection over Union (IoU) score of 64.46%, surpassing the X-Net model's score of 62.54%. Similarly, for Vertical-Vertical (VV) polarization, the U-Net model achieved an IoU score of 67.35%, outperforming the X-Net model's 64.38%. These results underscore the U-Net model's effectiveness in flood detection using radar imagery. However, it is essential to note that the U-Net model architecture used in [18] has not been altered. This raises the question of whether this specific U-Net architecture is the most appropriate choice for segmentation applications. A more thorough analysis is warranted in the context of SAR image segmentation, which presents unique complexities that necessitate specialized handling.

Based on the brief review of deep learning segmentation methods discussed earlier, this study aims to develop a robust CNN model for mapping floodwater. Specifically, it investigates the effects of fine-tuning different layers within a U-Net encoder as applied to SAR image segmentation. This paper presents a comprehensive investigation into enhancing floodwater mapping using machine learning techniques. The study employs a fine-tuned U-Net model to label flood-affected pixels in SAR imagery accurately. The results reveal that fine-tuning the first two blocks of the U-Net encoder achieved a remarkable IoU score of 78.904%, representing an improvement of 8.663% over baseline methods. This study demonstrates the proposed approach's efficacy in flood mapping and contributes valuable insights into the potential of machine learning for disaster management and climate resilience. Therefore, the main contributions of this paper are as follows:

- Exploring the impact of block-level fine-tuning in the encoder architecture of the U-Net model.
- Introducing an efficient SAR image segmentation approach for improved flood mapping.
- Providing foundational knowledge in remote sensing for flood mapping.
- Offering practical insights for future radar-based flood monitoring.
- Enhancing flood detection methods for improved climate resilience and disaster management.

https://doi.org/10.31436/iiumej.v26i1.3157

2. MATERIALS AND METHODS

2.1. Synthetic-Aperture Radar Imagery

Synthetic Aperture Radar images are produced by an active system that uses microwave signals transmitted to the ground and received back by a sensor platform, which can be either airborne (via planes) or satellite-based [17]. This process entails signal transmission, reception, and the application of specific filters, as illustrated in Figure 1.

In Vertical-Horizontal (VH) polarization, the transmitted signal's electric field is vertical, while the received signal is measured in both vertical and horizontal orientations. Vertical-vertical (VV) polarization, in which both the transmitted and received signals are oriented vertically.

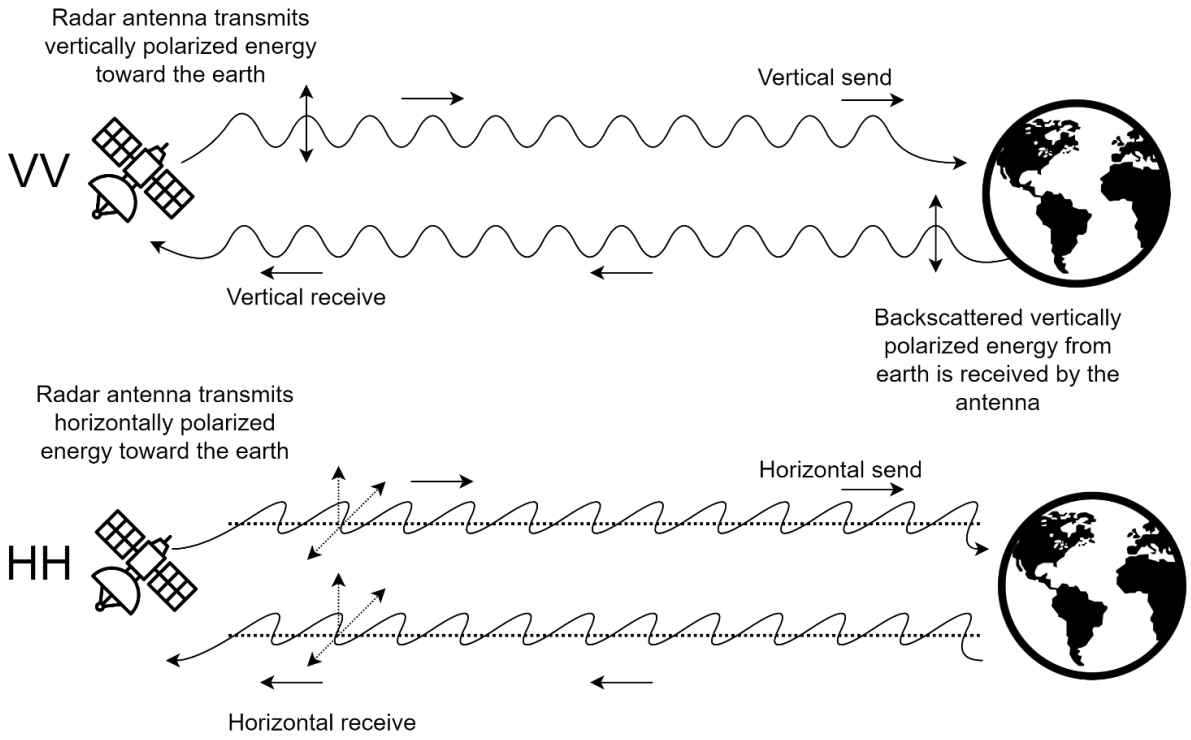

Figure 1. The first symbol indicates the direction of signal transmission, and the second indicates the direction of signal reception.

The complex interplay between transmitted signals and the terrain influences the distribution and reception of VH and VV data. Visual aids, such as figures, depict these interactions, illustrating how VH and VV signals interact with various surface features and water bodies. These visuals highlight signal fluctuations resulting from different polarization modes and surface characteristics, such as open water, vegetation, or urban environments. The advantages of SAR imagery include:

- Operation in various weather conditions, ensuring uninterrupted monitoring.
- Penetration of obstacles like clouds and vegetation, reflecting diverse surface features for insightful analysis.
- Provision of high-resolution images for precise flood area identification and land feature differentiation.

https://doi.org/10.31436/iiumej.v26i1.3157

2.2. Planetary Computer Data

The dataset for model training is accessed via the Planetary Computer, a platform hosted on Microsoft's Azure cloud infrastructure that provides a wide range of geospatial and environmental datasets. This platform provides a suite of cloud computing services for deploying, managing, and scaling applications and services globally, as detailed in [19]. The datasets available on this platform are freely accessible through the Data Catalog and come with accompanying metadata and code examples to facilitate their effective use.

Raw data from upstream data providers is initially transmitted to Azure Blob Storage, from which users can easily retrieve the data via HTTP requests. The Planetary Computer enhances accessibility by creating cloud-optimized data variants, including converting data into Cloud-optimized GeoTIFF format. Data exploration is facilitated through the STAC API, while a tile server visualizes data on maps using the Explorer tool. For a visual representation of the relationship between upstream data providers and the Planetary Computer, please refer to Figure 2.

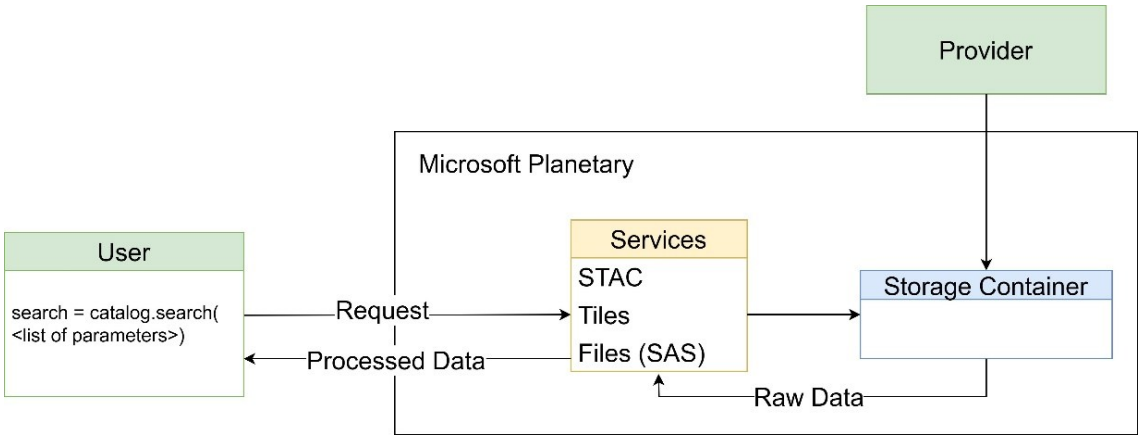

Figure 2. Relationship between upstream data providers, Planetary Computer and users.

2.3. Data Preprocessing

Accurate predictions hinge on the critical step of data preprocessing. Various data preprocessing strategies were employed to enhance classification performance and generate additional training data. The quality and utility of the training dataset were optimized through meticulous processes such as masking, augmentation, channel combination, and scaling.

2.3.1. Step 1 - Pixel Masking: Improving Data Quality

In the context of satellite imagery, pixel values indicate the energy reflected to the satellite. In some regions outside the satellite's coverage, missing data points may exist within the dataset's images. Each image in this dataset is associated with a GeoTIFF label, essentially serving as a binary mask. In these masks, a pixel value of 1 clearly indicates the presence of water, while a value of 0 signifies its absence. Notably, any missing or erroneous data is marked with a pixel value of 255. During the image loading phase for training, this issue is intelligently handled by converting any pixels labeled as missing data to represent the absence of water.

2.3.2. Step 2 - Data Normalization

Normalization involves scaling pixel values to achieve a standard scale and distribution. This technique enables the model to converge more quickly during training, often resulting in improved predictive performance. Pixel z-score normalization is carried out using Eq. (1):

https://doi.org/10.31436/iiumej.v26i1.3157

$$z = \frac{X-\mu}{\sigma} \quad (1)$$

where X represents the original pixel value while μ and σ denote the mean and standard deviation values of the pixel values across the entire image.

2.4. Data Augmentation

Utilizing data augmentation is a crucial machine-learning strategy aimed at mitigating overfitting during model training, as highlighted by [20]. In the field of computer vision, image augmentation methods have become a prominent implicit regularization technique for reducing overfitting in deep convolutional networks. These approaches are widely used to enhance performance, as emphasized in previous studies [20], [21], [22]. The necessity of data augmentation becomes clear in our efforts to develop a robust machine-learning model for radar-based flood mapping. This technique introduces variability into the training dataset, reflecting real-world complexities. This study applies various image data augmentation techniques, including random resized crops, horizontal and vertical flipping, rotations, and blurring, to the dataset. Augmentor, an image augmentation library for machine learning [23], is utilized to enhance radar imagery and its corresponding masks, thereby improving the accuracy of flood mapping. Figure 3 presents a visual representation of the data augmentation process.

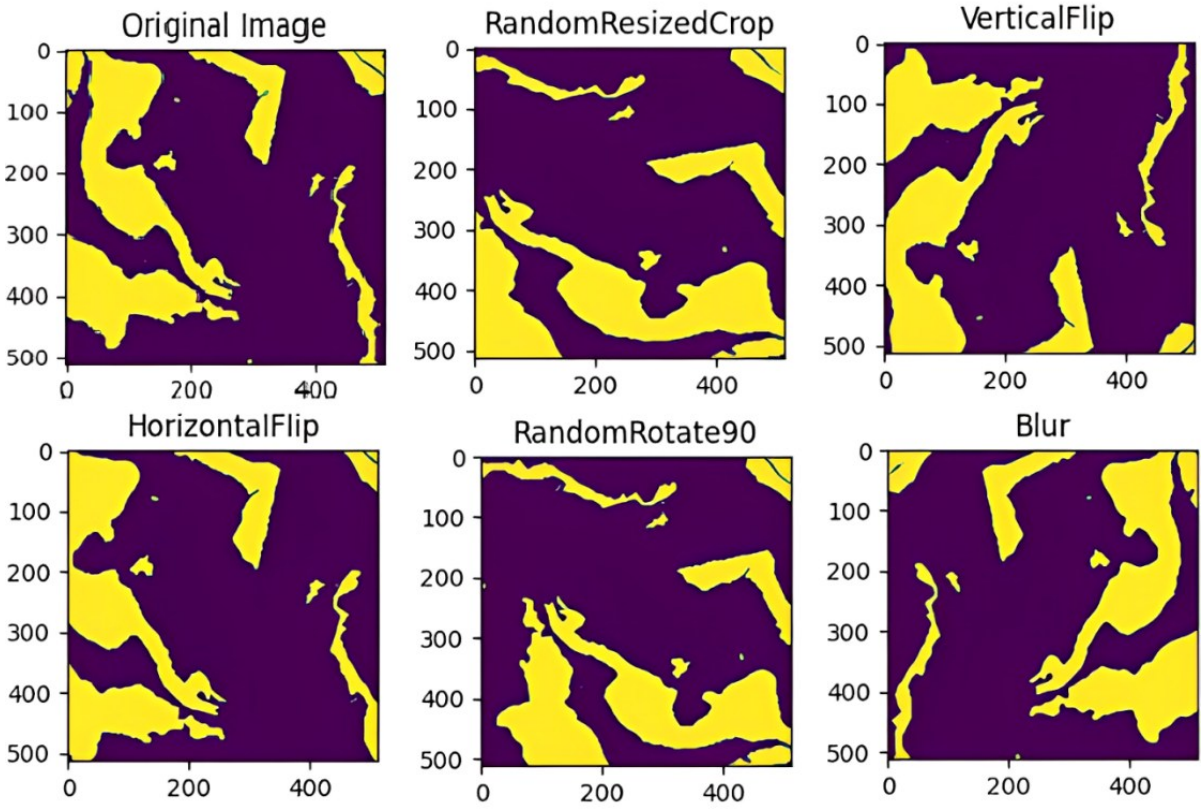

Figure 3. Visual representation of data augmentation results.

Random Resized Crop: The Random Resized Crop technique was incorporated to diversify the size and scale of radar images. This method randomly crops and resizes images to dimensions of 512x512 pixels, with scaling factors ranging from 0.75 to 1.0. By doing so, variations in the field of view of radar sensors are simulated, enhancing the model's adaptability to different spatial contexts.

https://doi.org/10.31436/iiumej.v26i1.3157

Vertical and Horizontal Flips: Vertical and horizontal flips were implemented to expose the model to variations in orientation. These augmentations create mirror images of the radar data, effectively doubling the dataset. They simulate different perspectives and orientations that radar sensors may encounter in real-world flood mapping scenarios.

Random 90-Degree Rotations: Random 90-degree rotations add rotational diversity to the training data. Flood events can manifest at *varIoUs* angles relative to the radar sensor. By incorporating these rotations, our model learns to recognize flood patterns from different orientations, bolstering its ability to map floods accurately under varied conditions.

Blurring: The blurring augmentation adds complexity to the dataset by mimicking radar imagery affected by adverse weather conditions or natural interference. Training on these blurred images makes the model more robust, improving its ability to identify flood-affected regions in radar images with lower clarity.

2.5. U-Net Architecture

In this study, the influential U-Net architecture [15] was utilized to facilitate the task of flood mapping. While the core architecture closely follows the original U-Net framework proposed in the seminal paper [18], specific adaptations were implemented to optimize its performance for radar-based flood mapping. The U-Net architecture comprises blocks, each containing two 3x3 convolutional layers with ReLU activation. These convolutional layers are essential for feature extraction and mapping. The network is organized into a series of blocks, each connected to the next through either a max-pooling or an upsampling operation (Figure 4). Transitioning from one block to the next involves scaling and compression operations. The final layer of our U-Net architecture consists of a 1x1 convolutional layer with a sigmoid activation function. This layer is crucial in mapping the feature vector to a continuous range between 0 and 1. During the evaluation phase, a threshold value of 0.5 was applied, allowing us to categorize pixels as follows:

- Pixels with values above 0.5 were designated as 1, indicating flood-affected regions.
- Pixels with values below 0.5 were classified as 0, signifying non-flood areas.

Notably, traditional transposed convolutional layers were replaced with a hybrid approach that combines bilinear upsampling followed by 2x2 convolutions. This method of upsampling with bilinear interpolation allows for improved capture of fine features [24]. Additionally, in the blocks designated for fine-tuning, 64 filters were incorporated, with their count doubled after each max-pooling operation to better capture complex patterns [25]. Conversely, after each upsampling operation, the number of filters was halved, leading to a more efficient computational process. This technique enhances the model's ability to capture intricate features while minimizing computational overhead.

https://doi.org/10.31436/iiumej.v26i1.3157

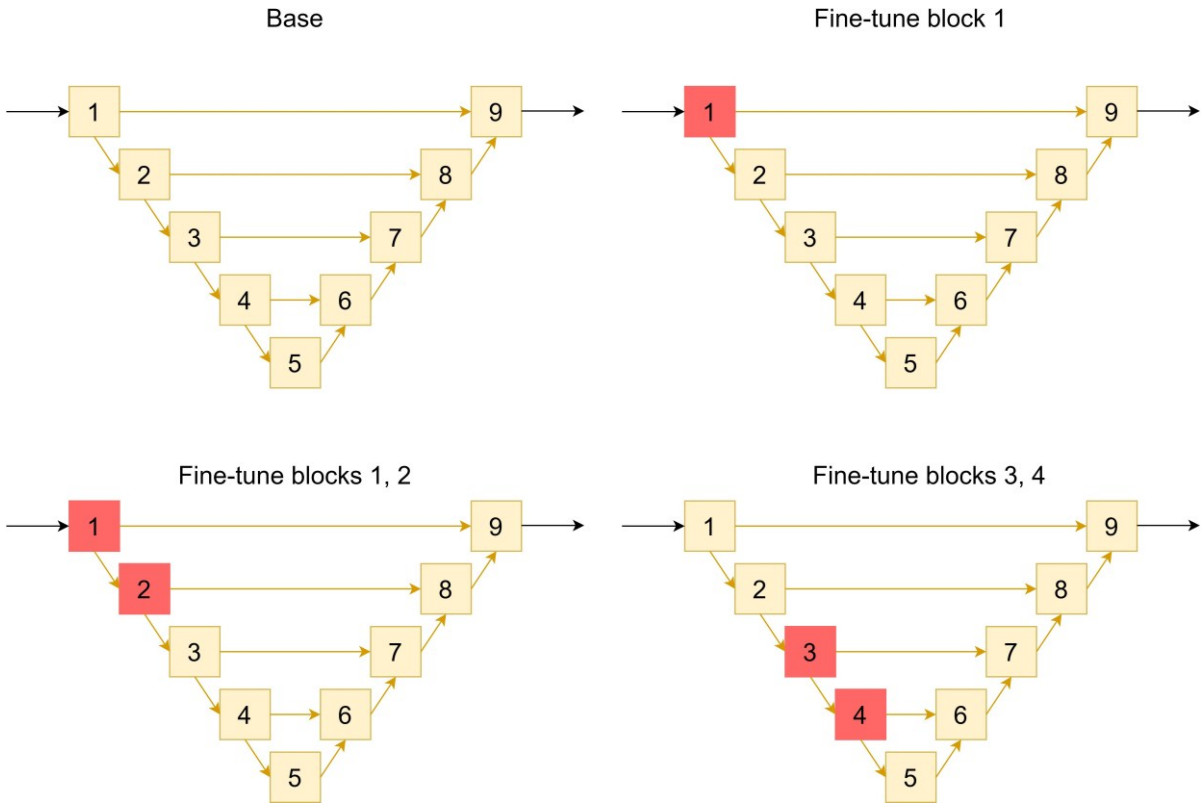

Figure 4. Schematic of the U-Net [18] and the fine-tuning strategies. Red blocks are the blocks included in fine-tuning, and yellow ones are frozen.

2.6. Stratified K-Fold Cross Validation

To ensure a robust evaluation of the models, Stratified K-Fold Cross-Validation (SKCV) was employed, an advanced technique that provides a fair and unbiased assessment of model performance [26]. SKCV meticulously divides our floodwater radar imagery dataset into K subsets, ensuring that each fold maintains a proportional representation of the various classes present in the data. This stratification is essential, particularly when dealing with imbalanced datasets where certain classes may be underrepresented. By preserving the class distribution in each fold, SKCV helps mitigate biases arising from uneven class proportions. The SKCV process involves the following steps:

Step 1 - *Dataset Division*: The floodwater radar imagery dataset, denoted as X, is divided into K subsets: $X_1, X_2, \ldots X_K$.

Step 2 - *Iterative Evaluation*: For each iteration i from 1 to K:

- Validation and Training Sets: One subset, X_i, is used as the validation set, while the remaining subsets are merged to form the training set.
- Model Training: Our machine learning models are trained on the training set, allowing them to learn patterns and relationships within the data.
- Model Evaluation: The trained models are evaluated on the validation set, providing specific performance metrics for each fold.

Overall model performance is assessed by averaging evaluation metrics across iterations. This is done by calculating the average performance metric P_{avg}, derived by summing

performance metrics P_i from each fold and dividing by the number of folds K, as shown in Eq. (2):

$$P_{avg} = \frac{1}{K}\sum_{i=1}^{K} P_i \quad (2)$$

This approach ensures that each class is evenly distributed across the K-folds, maintaining the sample distribution ratio among the classes within SKCV. It provides an unbiased evaluation of model performance by accurately representing the target class distribution in each fold.

2.7. Evaluation Metric: Intersection over Union

For precise model assessment, the Jaccard Index, also known as the Generalized Intersection over Union (IoU), was utilized. This metric is crucial for comparing ground truth and predicted segmentations in supervised segmentation models [27]. It measures label similarity, indicating the overlap between segmentations. Higher values indicate better alignment, while lower values signify less accurate segmentations. The mathematical formulation of the Jaccard Index is presented in Eq. (3):

$$IoU = \frac{|A \cap B|}{|A \cup B|} = \frac{|A \cap B|}{|A|+|B|-|A \cap B|} \quad (3)$$

where, A represents the set of flood pixels in the label, while B corresponds to the set of predicted flood pixels.

3. EXPERIMENTS

3.1. Dataset

In our study, the dataset used for both training and testing was sourced from the project described in [28]. This project provides a global catalog of flood maps for major historical events, accessible via Microsoft's Planetary Computer platform. The dataset used for flood detection in this study consists of high-resolution radar images captured by the Sentinel-1 satellite, which employs SAR technology. SAR is particularly effective for flood monitoring as it can capture images through clouds day and night, making it ideal for use in adverse weather conditions. The dataset contains images processed in dual polarization (VV and VH), which helps capture the flood extent more accurately. The thirteen most severe floods, determined by their peak water levels, were specifically selected, as shown in Table 1.

Table 1. List of the ten most severe flood events selected from a total of 156 simulated historic surge events documented in [28].

Name	Country	Date	Lat	Lon	Peak Water Level
Rosita	AU	21/04/2000	-18.2	122.26	8.42
Ingrid	AU	17/03/2005	-12.78	135.29	8.42
Chris	AU	07/02/2002	-19.85	120.41	8.19
Annette	AU	19/12/1994	-19.7	120.81	7.82
Orson	AU	24/04/1989	-20.66	116.7	6.45
Glenda	AU	31/03/2006	-20.76	116.62	6.38
Ian	AU	03/03/1992	-20.71	115.46	6.34
Vance	AU	24/03/1999	-21.8	114.74	6.2
Katrina	US	29/08/2005	27.7	-85.21	6.09
Connie	AU	20/01/1987	-20.31	118.58	5.99
Bobby	AU	27/02/1995	-20.78	116.67	5.91
Rachel	AU	08/01/1997	-20.31	118.57	5.85
John	AU	16/12/1999	-20.31	118.58	5.75

https://doi.org/10.31436/iiumej.v26i1.3157

The training dataset comprises 542 chips, totaling 1,084 images (each image paired with a corresponding label), facilitating supervised learning techniques. For a visual example of a chip and its corresponding water labels, refer to Figure 5. The radar images in the dataset are stored as GeoTIFF files, each containing 512x512 pixels. These images are measured in decibels (dB) and are acquired using the Sentinel-1 system, which employs a dual-polarization SAR technique. The SAR data is collected in both VV and VH polarizations, as shown in Figure 6. Depending on the specific flood detection requirements, one or both polarization bands are selectively used for analysis.

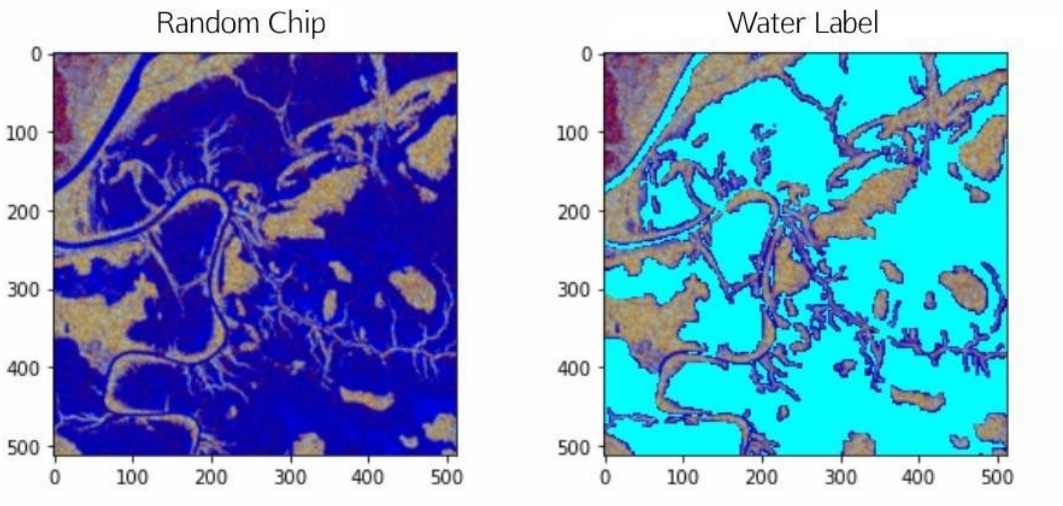

Figure 5. Visual representation of a random chip with its water labels.

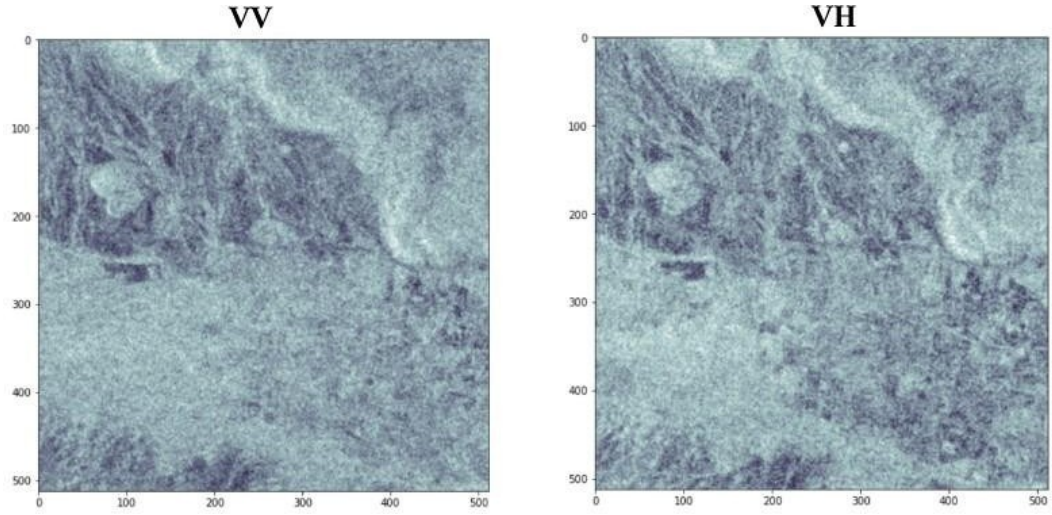

Figure 6. Visual comparison of VV and VH bands for polarization distinctions.

3.2. Experimental Design

It is important to note that including skip connections in the U-Net architecture complicates the conventional distinction between shallow and deep layers, necessitating a thorough investigation to determine the most effective fine-tuning strategy.

The U-Net encoder was divided into several subdivisions to tackle this challenge, each encompassing layers of varying depths. This division strategy is crucial for determining which network segments are most relevant for fine-tuning. The subdivisions are illustrated in Figure 4 and outlined as follows:

- Fine-Tuning the First Block (1): This experiment involved fine-tuning only the U-Net encoder's initial block.
- Fine-Tuning the First Two Blocks (1, 2): This experiment explored the impact of fine-tuning the encoder's first and second blocks.
- Fine-Tuning the Second Half of the Encoder (3, 4): This experiment focused on fine-tuning the latter part of the encoder, specifically blocks 3 and 4.

3.3. Experimental Setup

The experimental setup is the cornerstone of our research, detailing key elements such as the operating system, hardware, and software. The experiments were conducted on Ubuntu 20.04.1 LTS, utilizing an Intel Core i7 processor and an NVIDIA GeForce RTX 2080 Ti for high-performance computation. The exact package versions used are outlined in Table 2, ensuring accuracy and reproducibility. This carefully curated setup ensures seamless interactions, boosting reliability. Strategic environment configurations were applied to optimize efficiency and effectiveness, providing a solid foundation for comprehensive flood detection model evaluations.

Table 2. Imported packages and their descriptions

Package	Version	Description
albumentations	1.3.1	Image augmentation library for machine learning tasks.
catboost	1.2	Gradient boosting library optimized for categorical data.
gdal	3.4.1	Geospatial Data Abstraction Library for raster data manipulation.
matplotlib	3.6.2	Visualization library for creating static, animated, and interactive plots.
numpy	1.24.0	Fundamental package for scientific computing with Python.
pandas	1.5.2	Data manipulation and analysis library providing data structures and functions.
rasterio	1.3.8	Library for reading and writing geospatial raster data.
sklearn	1.2.0	Machine learning library with tools for classification, regression, and more.
tqdm	4.64.1	Library for reading and writing geospatial raster data.

3.4. Model Training

During the training process, the early stopping technique was applied. This technique halts training once the minimum loss is reached on the validation set and no improvement is observed for 20 consecutive epochs. The model that performed best on the validation set was saved for further evaluation on the test set. If early stopping did not occur within 200 epochs, the training was deemed unsuccessful, ensuring that resources were not wasted on unproductive runs.

The training was carried out using the configuration detailed in Table 3. All experiments employed the same folds to facilitate a meaningful comparison of different fine-tuning scenarios. The network's performance was consistently evaluated using the same test set, representing the entire held-out fold.

Table 3. Model training configuration

Parameters	Value
Optimization algorithm	ADAM optimizer
Loss function	Binary Cross-Entropy
Batch size	32
Learning rate	10−4

https://doi.org/10.31436/iiumej.v26i1.3157

4. RESULTS AND DISCUSSIONS

The results of the study reveal an interesting phenomenon. When comparing different fine-tuning strategies for the U-Net encoder, it was consistently observed that training the shallow path while freezing the deep path produced superior results (Figure 7). Notably, the shallow path contains significantly fewer parameters (Table 4), with approximately less than half the number found in the deep path (comparing the Blocks 1 and 2 scheme to Blocks 3 and 4). Despite this substantial difference in parameter count, training fewer parameters still improved performance.

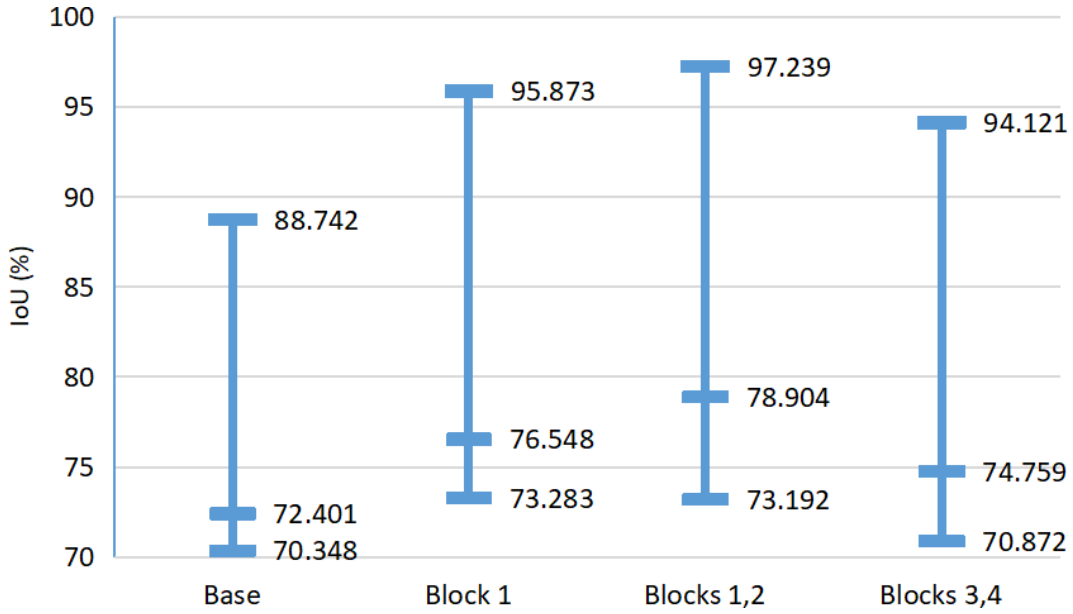

Figure 7. IoU scores for different fine-tuning schemes

Table 4. Mean IoU scores and number of parameters of different fine-tuning schemes

U-Net Model	Baseline	Block 1	Blocks 1,2	Blocks 3,4
Number of Parameters	3.1e+7	3.7e+5	2.5e+6	4.3e+7
Mean IoU (%)	70.241	76.548	78.904	74.759

As demonstrated in Table 4, our findings provide important insights into the efficiency of fine-tuning various blocks within the U-Net architecture for floodwater mapping. The maximum Intersection over Union (IoU) score of 78.904% obtained by fine-tuning the first two blocks of the encoder architecture is especially remarkable because it represents an 8.663% improvement above baseline approaches. This increase demonstrates the effectiveness of intentional model fine-tuning in enhancing performance for specific applications like flood detection. Several elements contribute to the U-Net model's performance:

Layer-Specific Fine-Tuning: By concentrating on fine-tuning only the first two blocks, these layers' extensive feature extraction capabilities were leveraged while preserving the stability of the deeper levels. This strategy lowered the danger of overfitting, which is common when fine-tuning deeper layers, while allowing for more efficient training with fewer parameters. The network's short route (with fewer parameters) produced better results, demonstrating that effective feature learning may occur without too complicated model designs.

Data Preprocessing and Augmentation: Preprocessing processes such as pixel masking, normalization, and other data augmentation approaches considerably enhanced the quality and variability of the training dataset. This variety enabled the model to generalize more well across various flood conditions, increasing its resilience in real-world applications.

Application of SAR Imagery: SAR imagery, recognized for its ability to pierce cloud cover and produce high-resolution data, enabled accurate flood mapping even in difficult climatic circumstances. The model's dependence on SAR data highlights the value of remote sensing in flood control, especially in locations where traditional ground-based surveillance is restricted.

Implications for Disaster Management: Our technique's improved mapping accuracy has important implications for disaster management and climate resilience. Improved flood mapping helps governments and humanitarian groups respond more quickly and precisely, allowing for improved resource allocation and focused relief operations. This expertise is critical for reducing the human and economic toll of flooding occurrences.

Future Directions: While the findings are encouraging, more studies are needed to investigate the use of the U-Net model in various flood situations and geographic locations. Furthermore, additional data sources, such as meteorological and hydrological information, may improve the model's forecasting powers. The possibility of real-time flood monitoring and evaluation might be a useful path for future research, leading to a more proactive approach to disaster management.

Our findings show that fine-tuning the U-Net architecture is a potent technique for floodwater mapping, with considerable gains in accuracy and efficiency. The findings provide a solid platform for future advances in remote sensing applications, underlining the importance of machine learning in solving global concerns such as climate change and natural catastrophes.

Figure 8 provides a comparison of segmentation results from several fine-tuning procedures used on a U-Net model for flood detection. Flood maps generated using the fine-tuning of Block 1 and Blocks 3, 4 techniques achieved IoU scores exceeding 74%, with the resulting flood maps showing similar patterns. However, the flood maps produced by the fine-tuned Blocks 1, 2 approach demonstrated greater precision, capturing finer details and aligning more closely with the ground truth labels, leading to the highest overall score.

The input data in the VH column comprises vertical-horizontal polarization (VH) from radar pictures, which were most likely collected using Synthetic Aperture Radar (SAR) devices. SAR data is very useful in flood mapping since it can pierce clouds and collect photos in all weather, making it excellent for estimating flood extents. This serves as the starting point for model projections.

The Label column depicts the ground truth, the manually labeled flood extent. It shows flooded areas in yellow and dry sections in deep purple, serving as a baseline for assessing the model's accuracy. The Base column displays the results of the base U-Net model with no fine-tuning. While the basic model covers the general flood size, the forecasts are less precise, with insufficient accuracy in identifying smaller features, which might be essential in flood detection jobs.

The subsequent columns, Block 1 and Blocks 1 and 2 display the results of fine-tuning various areas of the U-Net encoder. Fine-tuning Block 1 (the shallow layers) significantly increases accuracy, capturing more specific flood extents than the baseline model. Further fine-tuning using Blocks 1 and 2 further improves the findings, catching precise details of flood boundaries and producing the most accurate predictions. This strategy is most likely associated

with the greatest IoU score described before, highlighting the need for shallow layers for detailed flood mapping.

Finally, the findings in Blocks 3 and 4 demonstrate the effect of fine-tuning the U-Net encoder's deeper layers. While this method captures wider flood patterns, it ignores the fine-grained intricacies apparent in forecasts from fine-tuning superficial layers. These findings indicate that deeper layers are less successful at recording accurate flood limits than shallow ones. Overall, the comparison shows that focusing on fine-tuning the shallower regions of the network results in more accurate flood extent identification, especially when collecting finer details.

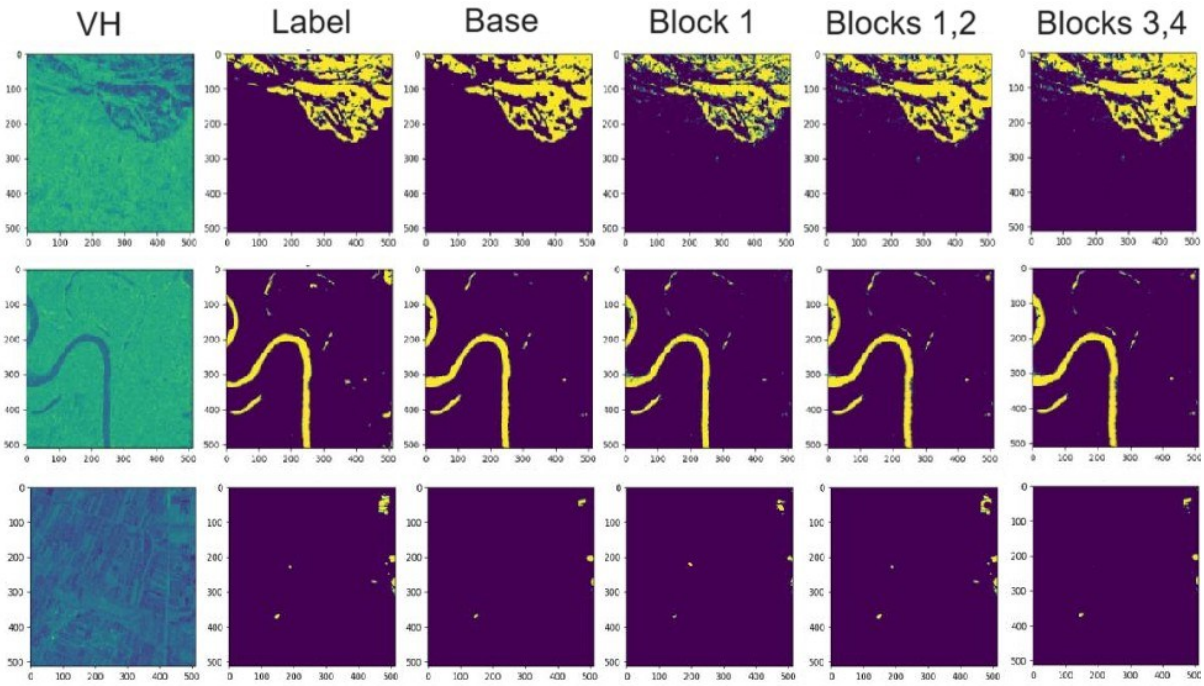

Figure 8. Visual comparisons of flood detection results for the different fine-tuning schemes are shown, with yellow representing flood extents and deep purple indicating dry areas.

5. CONCLUSION, LIMITATIONS AND FUTURE WORKS

This paper has presented a comprehensive comparative analysis of fine-tuning various blocks within the U-Net encoder framework for flood extent detection. Our findings demonstrate that fine-tuning Blocks 1 and 2 outperformed other methods, yielding a more robust and efficient solution for flood mapping, with the highest IoU score of 78.904%. This systematic approach shows significant potential for improving flood mapping accuracy. Despite the promising results, limitations exist, including the reliance on a relatively small dataset of 13 flood events and the exclusive use of Sentinel-1 radar data, which may limit the model's generalization and real-time applicability in regions with less frequent data availability. Future research should concentrate on increasing the dataset, including other data sources like optical or LiDAR imaging, and investigating more complex structures like transformers or hybrid models. Furthermore, real-time implementation on cloud platforms and cooperation with disaster management organizations might increase the model's practical influence in real-world disaster response situations, boosting worldwide flood preparedness and mitigation.

REFERENCES

[1] L. P. Hoang et al., "Managing flood risks in the Mekong Delta: How to address emerging challenges under climate change and socioeconomic developments," Ambio, vol. 47, pp. 635–649, 2018, [Online]. Available: https://api.semanticscholar.org/CorpusID:3508948.

[2] M. Marchand, D. Pham, and T. Le, "Mekong Delta: Living with Water, But for How Long?," Built Environ., vol. 40, 2014, doi: 10.2148/benv.40.2.230.

[3] M. Tanguy, K. Chokmani, M. Bernier, J. Poulin, and S. Raymond, "River flood mapping in urban areas combining Radarsat-2 data and flood return period data," Remote Sens. Environ., vol. 198, pp. 442–459, 2017, doi: 10.1016/j.rse.2017.06.042.

[4] M. J. Hammond, A. S. Chen, S. Djordjević, D. Butler, and O. Mark, "Urban flood impact assessment: A state-of-the-art review," Urban Water J., vol. 12, no. 1, pp. 14–29, 2015, doi: 10.1080/1573062X.2013.857421.

[5] F. Dottori, G. Di Baldassarre, and E. Todini, "Detailed data is welcome, but with a pinch of salt : Accuracy, precision, and uncertainty in flood inundation modeling," Water Resour. Res., vol. 49, no. 9, pp. 6079–6085, 2013, doi: 10.1002/wrcr.20406.

[6] L. C. Smith, "Satellite remote sensing of river inundation area, stage, and discharge: a review," Hydrol. Process., vol. 11, pp. 1427–1439, 1997, [Online]. Available: https://api.semanticscholar.org/CorpusID:46008875.

[7] L. Pulvirenti, M. Chini, N. Pierdicca, L. Guerriero, and P. Ferrazzoli, "Flood monitoring using multi-temporal COSMO-SkyMed data: Image segmentation and signature interpretation," Remote Sens. Environ., vol. 115, pp. 990–1002, 2011, doi: 10.1016/j.rse.2010.12.002.

[8] L. Giustarini, R. Hostache, P. Matgen, G. J.-P. Schumann, P. D. Bates, and D. C. Mason, "A Change Detection Approach to Flood Mapping in Urban Areas Using TerraSAR-X," IEEE Trans. Geosci. Remote Sens., vol. 51, no. 4, pp. 2417–2430, 2013, doi: 10.1109/TGRS.2012.2210901.

[9] Y. Jia et al., "Caffe: Convolutional Architecture for Fast Feature Embedding," Proc. 22nd ACM Int. Conf. Multimed., 2014, [Online]. Available: https://api.semanticscholar.org/CorpusID:1799558.

[10] A. Gebrehiwot, L. H. Beni, G. Thompson, P. Kordjamshidi, and T. E. Langan, "Deep Convolutional Neural Network for Flood Extent Mapping Using Unmanned Aerial Vehicles Data," Sensors (Basel)., vol. 19, 2019, [Online]. Available: https://api.semanticscholar.org/CorpusID:91187268.

[11] E. Nemni, J. Aylett-Bullock, S. Belabbes, and L. Bromley, "Fully Convolutional Neural Network for Rapid Flood Segmentation in Synthetic Aperture Radar Imagery," Remote. Sens., vol. 12, p. 2532, 2020, [Online]. Available: https://api.semanticscholar.org/CorpusID:221980528.

[12] J. Yosinski, J. Clune, Y. Bengio, and H. Lipson, "How transferable are features in deep neural networks?" 2014.

[13] M. Divya, V. Chandran, D. J. Anitha, M. Anusree, and M. G. Nair, "Deep Learning-Based Flood Detection System Using Semantic Segmentation," 2024 7th Int. Conf. Circuit Power Comput. Technol., vol. 1, pp. 1584–1592, 2024, [Online]. Available: https://api.semanticscholar.org/CorpusID:272711335.

[14] D. Amitrano, G. Di Martino, A. Di Simone, and P. Imperatore, "Flood Detection with SAR: A Review of Techniques and Datasets," Remote Sens., vol. 16, no. 4, pp. 1–38, 2024, doi: 10.3390/rs16040656.

[15] O. Ronneberger, P. Fischer, and T. Brox, "U-Net: Convolutional Networks for Biomedical Image Segmentation," ArXiv, vol. abs/1505.0, 2015, [Online]. Available: https://api.semanticscholar.org/CorpusID:3719281.

[16] K. Sarra and A. Boulmerka, "Semantic segmentation of remote sensing images using U-net and its variants : Conference New Technologies of Information and Communication (NTIC 2022)," 2022 2nd Int. Conf. New Technol. Inf. Commun., 2022, doi: 10.1109/ntic55069.2022.10100581.

[17] R. K. Vincent, "RADAR | Synthetic Aperture Radar (Land Surface Applications)," null, 2015,

doi: 10.1016/b978-0-12-382225-3.00331-5.
[18] M. Abbasi, R. Shah-Hosseini, and M. Aghdami-Nia, "Sentinel-1 Polarization Comparison for Flood Segmentation Using Deep Learning," Proceedings, vol. 87, no. 1, 2023, doi: 10.3390/IECG2022-14069.
[19] P. Herath, "Azure Cloud Security for Absolute Beginners: Enabling Cloud Infrastructure Security with Multi-Level Security Options," Azur. Cloud Secur. Absol. Beginners, 2022, [Online]. Available: https://api.semanticscholar.org/CorpusID:244780408.
[20] C. Shorten and T. M. Khoshgoftaar, "A survey on Image Data Augmentation for Deep Learning," J. Big Data, vol. 6, no. 1, 2019, doi: 10.1186/s40537-019-0197-0.
[21] A. Mikołajczyk and M. Grochowski, "Data augmentation for improving deep learning in image classification problem," 2018 Int. Interdiscip. PhD Work., pp. 117–122, 2018, [Online]. Available: https://api.semanticscholar.org/CorpusID:49348179.
[22] S. Yang, W.-T. Xiao, M. Zhang, S. Guo, J. Zhao, and S. Furao, "Image Data Augmentation for Deep Learning: A Survey," ArXiv, vol. abs/2204.0, 2022, [Online]. Available: https://api.semanticscholar.org/CorpusID:248240105.
[23] M. D. Bloice, C. Stocker, and A. Holzinger, "Augmentor: An Image Augmentation Library for Machine Learning," CoRR, vol. abs/1708.0, 2017, [Online]. Available: http://arxiv.org/abs/1708.04680.
[24] L. Xu, J. Xu, Q. Zheng, J. Yuan, and J. Liu, "A miniature U-net for k -space-based parallel magnetic resonance imaging reconstruction with a mixed loss function," Quant. Imaging Med. Surg., vol. 12, no. 9, 2022, [Online]. Available: https://qims.amegroups.org/article/view/96423.
[25] W. Shang, K. Sohn, D. Almeida, and H. Lee, "Understanding and Improving Convolutional Neural Networks via Concatenated Rectified Linear Units," in Proceedings of The 33rd International Conference on Machine Learning, 2016, vol. 48, pp. 2217–2225, [Online]. Available: https://proceedings.mlr.press/v48/shang16.html.
[26] S. Widodo, H. Brawijaya, and S. Samudi, "Stratified K-fold cross validation optimization on machine learning for prediction," Sink. J. dan Penelit. Tek. Inform., 2022, doi: 10.33395/sinkron.v7i4.11792.
[27] D. Ogwok and E. M. Ehlers, "Jaccard Index in Ensemble Image Segmentation: An Approach," in Proceedings of the 2022 5th International Conference on Computational Intelligence and Intelligent Systems, 2023, pp. 9–14, doi: 10.1145/3581792.3581794.
[28] "Planetary computer and Deltares global data," 2021.